Effect of the Drawing Process on the Wet Spinning of Polyacrylonitrile Fibers in a System of Dimethyl Sulfoxide and Water

Yan-Xiang Wang, Cheng-Guo Wang, Yu-Jun Bai, Zhu Bo

Carbon Fiber Center, College of Materials Science and Engineering, Shandong University, Jinan 250061, People's Republic of China

Received 1 February 2005; accepted 27 April 2006
DOI 10.1002/app.24793
Published online in Wiley InterScience (www.interscience.wiley.com).

ABSTRACT: The effect of the drawing process on the structural characteristics and mechanical properties of polyacrylonitrile (PAN) fibers was comparatively studied. The protofibers extruded from the spinneret were the initial phase of stretching, which involved the deformation of the primitive fiber with the concurrent orientation of the fibrils. Wet-spun PAN fibers observed by scanning electron microscopy exhibited different cross-sectional shapes as the draw ratio was varied. X-ray diffraction results revealed that the crystalline orientation of PAN fibers increased with increasing draw ratio; these differences in the orientation behaviors were attributed to the various drawing mechanisms involved. The crystalline and amorphous orientations of the PAN fibers showed different features; at the same time, the tensile properties were strongly dependent on the draw ratio. However, the stream stretch ratio had most influence on the tensile strength and the orientation of PAN fibers for the selected process parameters. Electron spin resonance proved that the local morphology and segmental dynamics of the protofibers were due to a more heterogeneous environment caused by the sequence structure. Differential scanning calorimetry indicated that the size and shape of the exotherm and exoenergic reaction were strongly dependent on the morphology and physical changes occurring during fiber formation. J Appl Polym Sci 104: 1026–1037, 2007

Key words: crystal structures; fibers; morphology; X-ray

INTRODUCTION

In recent years, there has been a growing interest in the study of making carbon fibers; this can be ascribed to an increasing need for high-quality fibers and the aim to produce these fibers with high economic efficiency.[1–3] It is well known that the properties of final carbon fibers are determined by a combination of the natures of the precursor fibers.[1] Polyacrylonitrile (PAN)-based carbon fibers have the advantages of lower cost and mature technology; therefore, PAN precursors are presently believed to be the most suitable and important precursors for the production of high-performance carbon fibers.[4–7] There have been a lot of methods for producing high-quality precursors, including drying spinning, dry-jet spinning, and wet spinning. Wet spinning is one of the main methods for the production of high-performance PAN precursors;[4] the mechanism of PAN-fiber formation by the wet-spinning technique is quite complex. The spinnability is effected by the properties of the spinning solution and by the coagulation bath conditions on wet spinning; various factors that influence the coagulation process include polymer composition,[8–12] molecular weight and distribution,[13–21] coagulation bath composition,[22–26] coagulation bath temperature,[27–31] and minus jet stretch.[32] Despite numerous studies on the fabrication and industrialization of produced PAN fibers, the molecular orientation of fiber materials obtained through the drawing process governs its properties, particularly the mechanical properties. A high degree of orientation produces high-filament-tenacity material; accordingly, the drawing process has been one of the most important procedures used to fabricate carbon fiber precursors. In this study, the drawing effect on the morphological features, crystalline structure, molecular orientation, and thermal and mechanical properties of PAN fibers were comparatively investigated; also, the effect of the stretch ratios on the structural properties of PAN fibers produced by wet spinning was examined.

Correspondence to: Y. X. Wang (wyx079@sdu.edu.cn).
Contract grant sponsor: National 863 Project; contract grant number: 2002AA304130.

Journal of Applied Polymer Science, Vol. 104, 1026–1037 (2007)

EXPERIMENTAL

Materials

Acrylonitrile (AN; Tianjin Chemical Reagent Plant, Tianjin, China) was distilled at 76–78°C before use;

TABLE I
Fixed Spinning Conditions

Spinning line position	Spinning conditions	Selected parameters	Drawing ratio
I coagulation bath (a)	Composition (DMSO/H_2O)	70/30	
	Temperature (°C)	60	
	Immersion length (cm)	100	
	First take-up roller speed (cm/min)	157	
II bath (b)	Composition (DMSO/H_2O)	30/70	
	Temperature (°C)	65	
	Immersion length (cm)	80	
	Second take-up roller speed (cm/min)	235.5	$\lambda_1 = V_2/V_1 = 1.5$
III bath (c)	Composition (DMSO/H_2O)	0/100	
	Temperature (°C)	100	
	Immersion length (cm)	80	
	Third take-up roller speed (cm/min)	350	$\lambda_2 = V_3/V_2 = 1.5$
Fourth washing bath (d)	Deionized water		
	Temperature (°C)	60	
	Fourth take-up roller speed (cm/min)	420	$\lambda_3 = V_4/V_3 = 1.2$
Fifth boiling drawing bath (e)	Deionized water		
	Temperature (°C)	100	
	Fourth take-up roller speed (cm/min)	798	$\lambda_4 = V_5/V_4 = 1.9$
Sixth drying and densing roller (f)	Five different heating rollers from 110 to 150°C	877	
	Fifth take-up roller speed (cm/min)		$\lambda_5 = V_6/V_5 = 1.1$
	Controlled pressure (MPa)	0.45–0.5	
Seventh stream-drawing machine (g)	Temperature (°C)	134–150	
	Sixth take-up roller speed (cm/min)	2370	$\lambda_6 = V_7/V_6 = 2.7$

V_1, First take-up roller speed; V_2, Second take-up roller speed; V_3, Third take-up roller speed; V_4, Fourth take-up roller speed; V_5, Fifth take-up roller speed; V_6, Sixth take-up roller speed; V_7, Seventh take-up roller speed.

itaconic acid (Lucky Co., Ltd., Chuolchome Ueda, Japan) was used as the second monomer. Azodiisobutyronitrile (Shandong Xueyin Chemical Fiber Co., Zibo, China) was used as an initiator; and dimethyl sulfoxide (DMSO; Shanxi Taigu Chemical General Plant, Taigu, China) was used as the solvent.

Spinning dope and its preparation

The free-radical solution copolymerization of itaconic acid and AN was carried out in a 20-L pilot-scale stainless reactor (Weihai Chemical Machinery, Shandong, China) with DMSO as a solvent and azodiisobutyronitrile as an initiator. The resulting polymer solution could be directly used as the spinning dope after the removal of excess solvent and unreacted monomers; the concentration and the molecular weight of the purified polymers in the dope were controlled at 21 wt % and 160,000, respectively.

Spinning conditions and fiber formation

The supply lines were provided with heat jackets to keep the solution at the desired temperature of 60°C; the spinneret used in this experiment had 1000 holes, the diameter of which was 0.06 mm (length/diameter = 1.2). The distances from hole to hole were very accurately uniform. The length of the coagulation bath was 180 cm, and the width and depth of the bath were 20 and 40 cm, respectively. For the maintenance of a uniform solvent concentration over the bath length, an aqueous solution of the bath was circulated by the circulation pump. To avoid the possibility of interference by heat-transfer phenomena, the coagulation bath was maintained at 60°C. The spinning conditions used in this experiment are given in Table I, the selected fibers were made from processes a–g. The concentration of DMSO in different baths was measured with a refraction apparatus.

Measurement

Scanning electron microscopy (SEM) observation of the precursors

The resultant polymers and fibers were examined with a Hitachi model 8010 scanning electron microscope (Tokyo, Japan) at an accelerating potential of 25 kV. To observe the cross-section of the obtained

TABLE II
Effect of Apparent Minus Stretch on the Property of As-Spun Fibers

Minus stretch (%)	Shape of cross-section of the protofiber	Tensile strength (cN/dtex)	Density (g/cm^3)
−55	Dumbbell	0.592	1.144
−50	Bean	0.586	1.142
−40	Oval	0.566	1.139
−30	Round	0.543	1.133
−20	Round	0.541	1.130

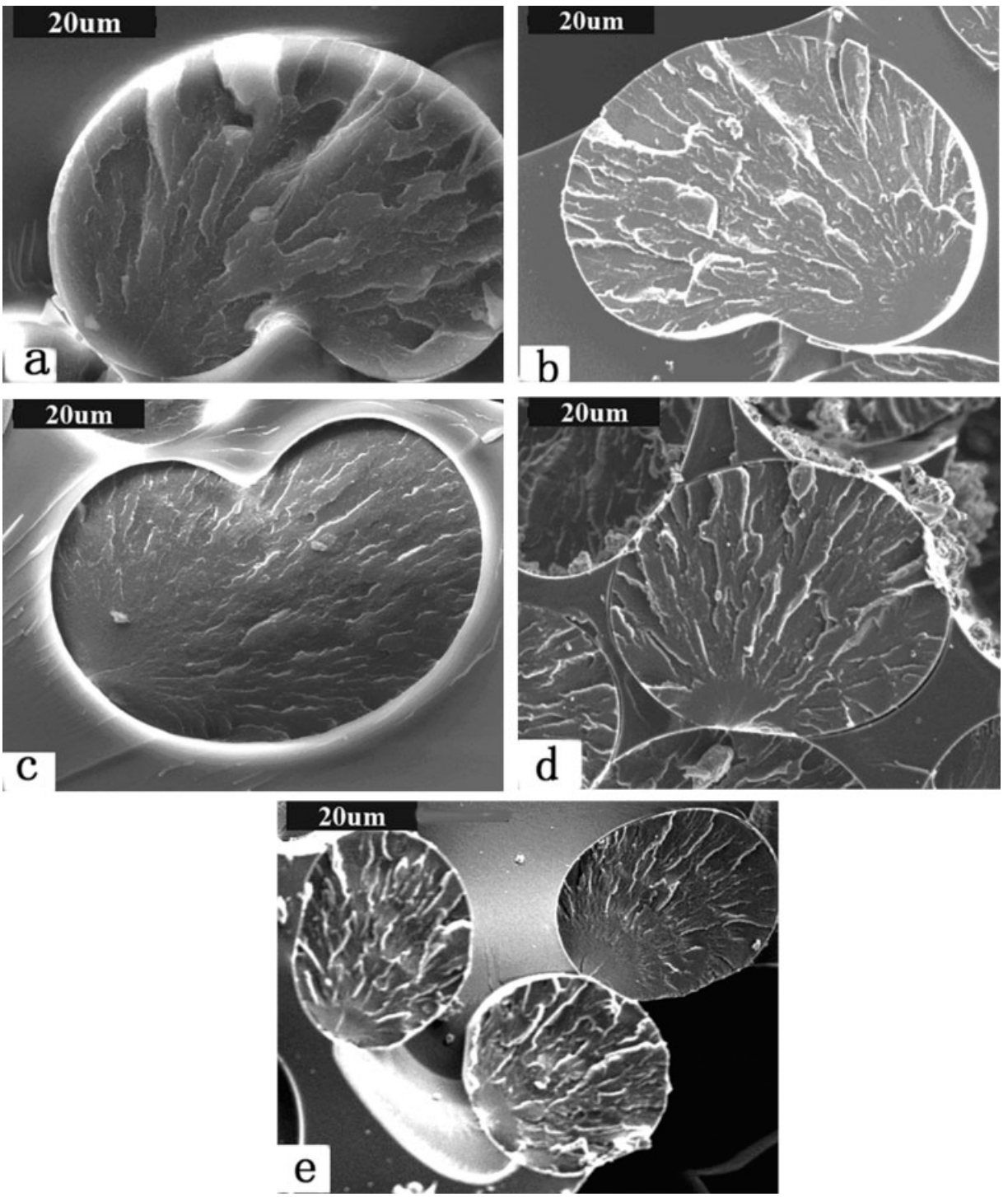

Figure 1 Effect of the apparent minus stretch on the morphology of as-spun fibers (coagulation bath temperature = 60°C, concentration = 60%).

precursors with different ratios and different coagulation temperatures, the coagulated fibers were directly immersed into liquid and subjected to lyopholization. The specimens were sputtered with gold to get a better avoid electron-charging effects with a metal-evaporating apparatus (fine-coat ion sputter JFC-1100, Jeol, Ltd., Tokyo, Japan).

Swelling degree

The swelling degree was obtained according to the following method: free water was removed from the swelling fibers with a centrifugal dehydrator at 3000 rpm for 15 min. The fibers were weighed (w), dried with a hot-air dryer at 110°C for 2 h, and

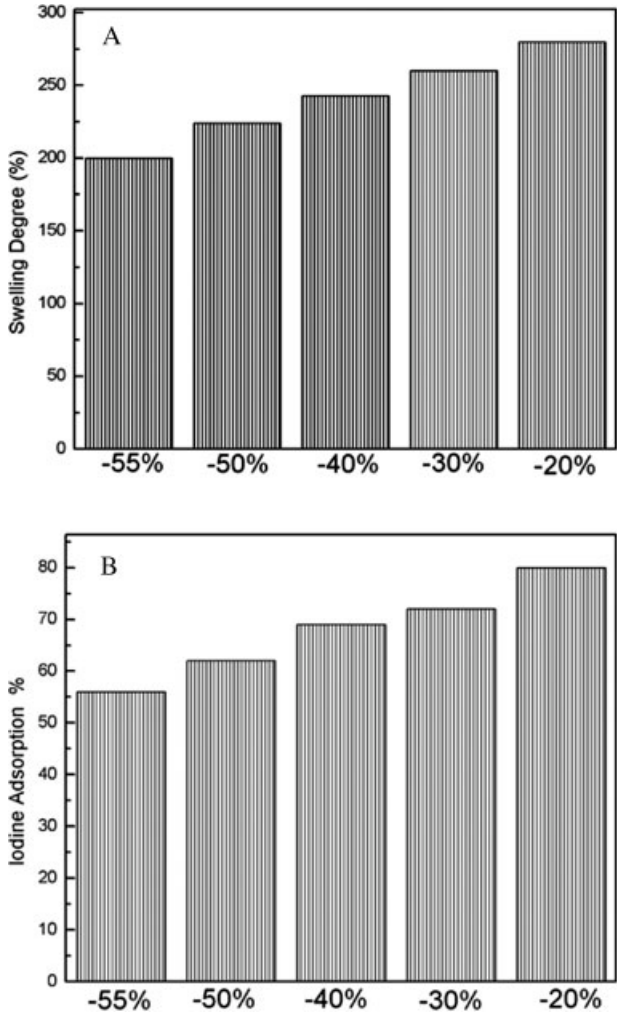

Figure 2 Effect of (a) swelling degree and (b) iodine adsorption on the morphology of as-spun fibers at different minus stretch ratios (coagulation bath temperature = 60°C, concentration = 60%).

weighed again (w_0). The swelling degree (S) was obtained from the following formula:

$$S(\%) = (w - w_0) \times 100/w_0$$

We calculated the different ratios (R_i's) of the swelling degree of the drawn fibers (S_i) to the swelling degree of the first coagulated fibers (S_f):

$$R_i = S_i/S_f$$

Iodine adsorption

The difference in lightness (ΔL) due to iodine adsorption was measured as described next. The dried precursors with different ratios were cut into lengths of about 6 cm and put in a 200-mL Erlenmeyer flask with a polished stopper, and 100 mL of iodine solution was added to the flask (we obtained the iodine solution by putting 50.76 g of iodine, 10 g of 2,4-dichlorophenol, 90 g of acetic acid, and 100 g of potassium iodide into a 1-L measuring flask and dissolving the mixture by adding water to bring the volume up to 1000 mL). The mixture was shaken at 60°C for 50 min for the adsorption treatment. The sample adsorbed iodine was washed in running water for 30 min and centrifuged for dehydration. The dehydrated sample was dried in air for 2 h. The dewatered fibers were put in the flask with 200 mL of DMSO liquid at 60°C; then, we carried out the potentiometer titration with an equivalent number of 0.01N of a silver nitrate and water solution. The samples with and without adsorbed iodine were parallel in the fiber direction, and crystallite size (L) values were measured by a Heter color difference meter (Leitz, Germany) simultaneously, with the L value of the sample without iodine adsorbed as L_1 and that of the sample with iodine adsorbed as L_2. The difference of L values ($L_1 - L_2$) was adopted as ΔL due to iodine adsorption.

X-ray diffraction (XRD)

A Rigaku X-ray diffractometer (D/MAX-rA, Tokyo, Japan) with Ni-filtered Cu Kα radiation as the source was used to study the wide angle at 40 kV and 60 mA. The sample was in disc form, which was prepared by the compression of the randomly aligned short fibers. Then, the crystalline-related properties of the sample were measured. The scanning speed was 6°C/min, and the scanning step was 0.02°.

The crystallinity (C) was calculated with the following equation:

$$C = S_c/S_t \times 100\% = S_c/(S_a + S_c) \times 100\%$$

where S_t is the total peak area, S_a is the amorphous peak area, and S_c is the crystalline peak area. The crystal size was calculated with the following equation:

$$L = K\lambda/(\beta \cos \theta)$$

where λ (the wavelength of X-rays used) = 1.541 Å, K is the Scherrer constant (0.89 was used), and β (arc) is the half-value width at 2θ = 17°.

Measurement of the spectra

The electron spin resonance (ESR) spectra were recorded on a Bruker ER-200D X-band spectrometer (Bruker, Germany) operating at a 100-kHz modulation, which was interfaced to an IBM-compatible PC to allow for acquisition of the spectra. The spectra of the samples were measured with a microwave power of 0.998000 μW, a modulation of 0.2000mT, a sweep width of 20mT, a sweep time of 1.0 min, amplitudes of CH1 = 200.0 and CH2 = 2.0, time constants of CH1 = 0.3 and CH2 = 0.03 s, and receiver modes of CH1

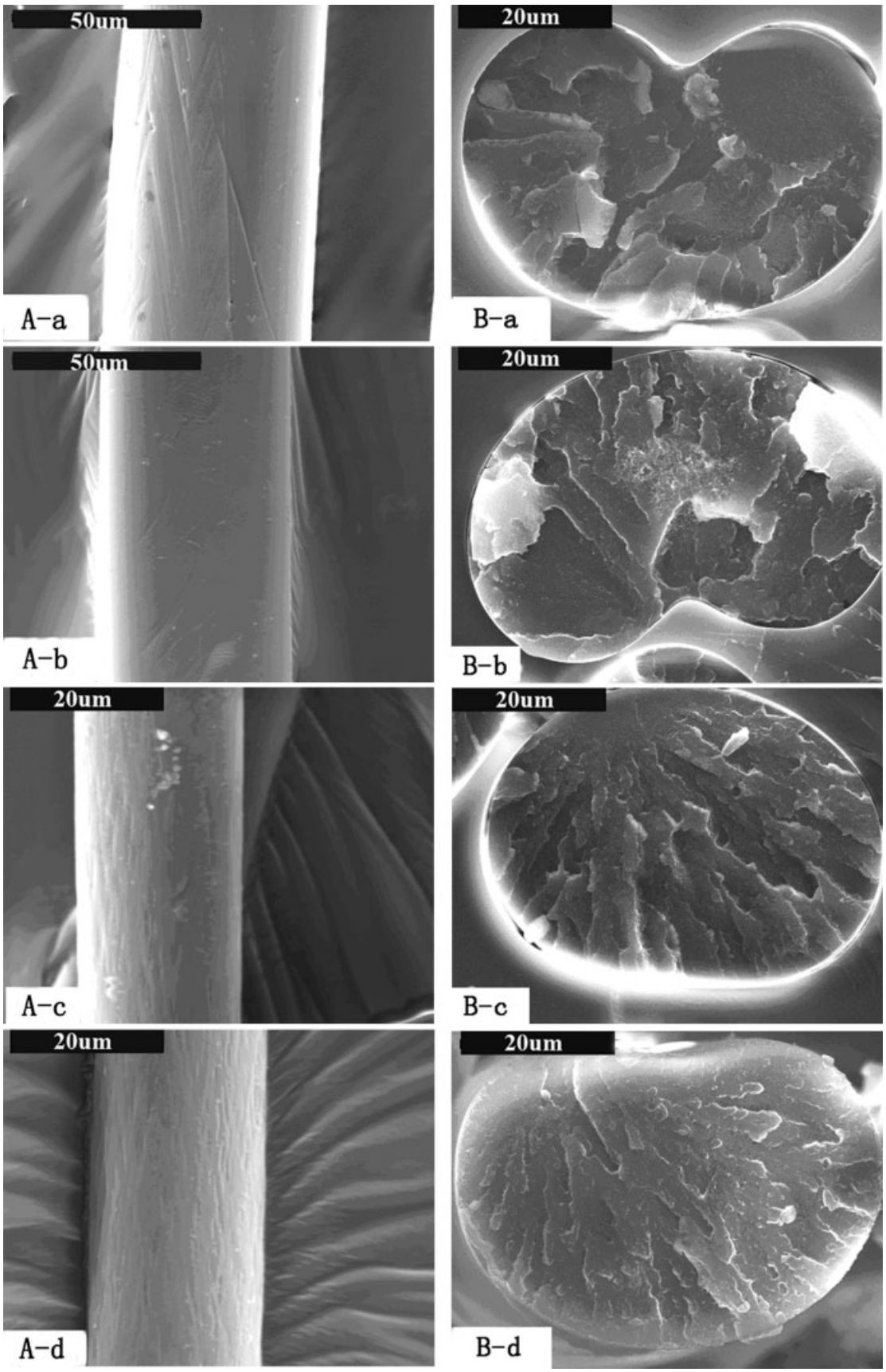

Figure 3 SEM micrographs of the (A) longitudinal sections and (B) cross-sections of wet-spun fibers.

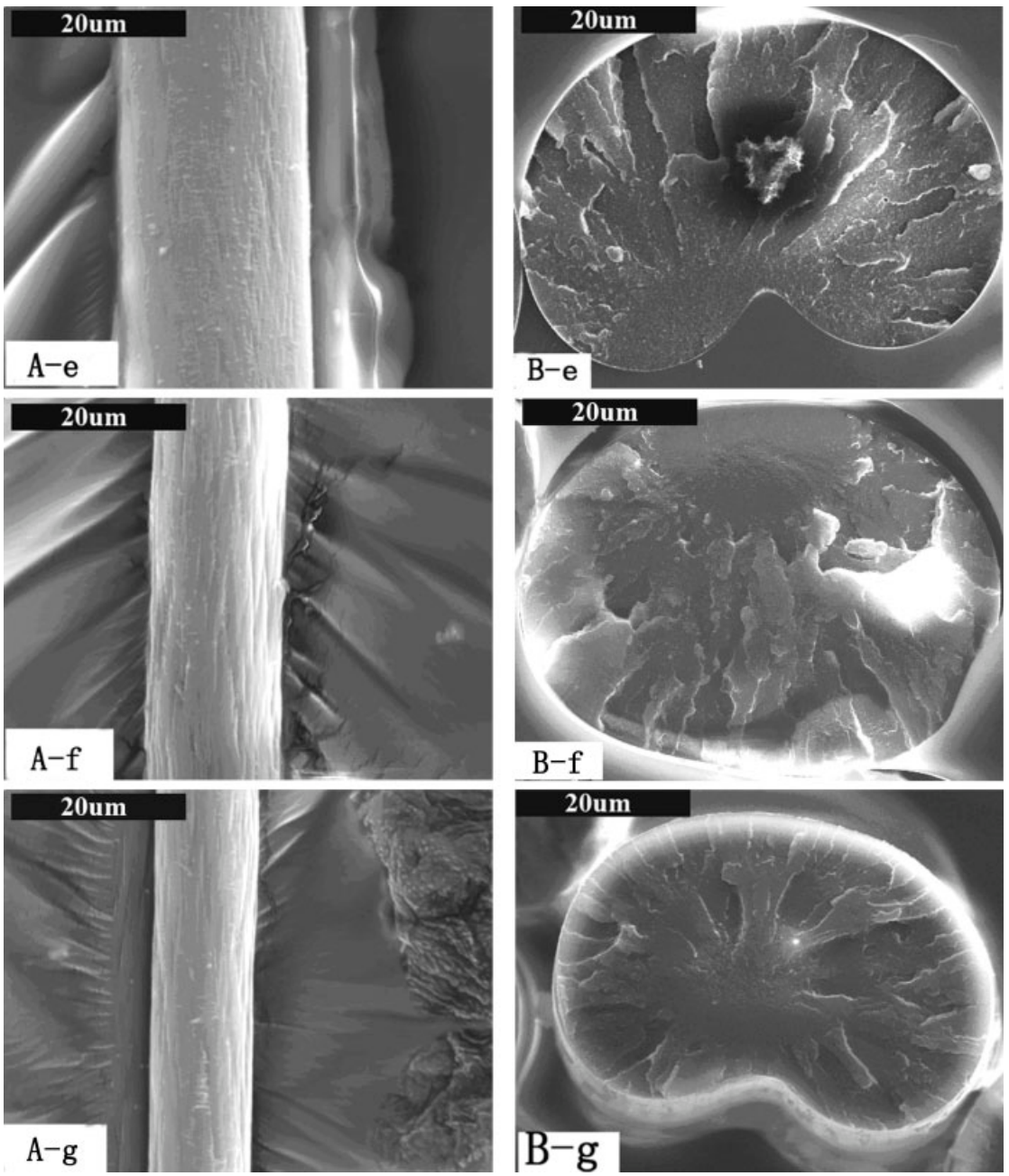

Figure 3 (*Continued from the previous page*)

= first and CH2 = second. The concentration of the radicals in the samples was 320.916 mT, which was calculated by double integration of the recorded spectra with 100-kHz modulation of the Zeeman magnetic field as the first modulation and comparison of the resulting absorption peak areas with that for a Varian pitch standard recorded at the same temperature.

Differential scanning calorimetry (DSC) analysis

A PerkinElmer DSC-41 thermal analyzer (Boston, MA) was used to perform DSC studies with about 4 mg of sample at a heating rate of 10°C/min under a nitrogen atmosphere.

Mechanical properties

The linear densities of the protofibers or fibers at different stretch stages were determined as the weight of 1-m long sections in milligrams; these were weighed on a physical scale balance.

The bulk density of the fibers was determined by means of a density gradient column maintained at 25°C. The columns were prepared in 250-mL graduated cylinders. Carbon tetrachloride with a density

of 1.57 g/cm^3 was first introduced into the column. We then slowly added xylene with a density of 0.90 g/cm^3 to the column, carrying out the plotting of the density of the calibrated floats against the position opposite the graduated scale of the column. We prepared the fiber samples for density determination by tying knots in the filaments and placing them in the column; the fibers first sunk and then came to rest at the position corresponding to their density.

The titer was measured with a XD-1 fiber fineness machine; all of the fibers were measured with an XQ-1 testing machine (both XD-1 and XQ-1 were made at Donghua University, Shanghai, China) at a crosshead speed of 0.5 mm/min with a testing length of 20 mm and a load cell of 15 g. In each case, at least 30 sample filaments were tested, and the average of 30 filaments was taken in each experiment.

RESULTS AND DISCUSSION

Effect of jet stretch minus rate

The ease of fiber formation under continuous spinning conditions was decided by jet stretch minus ratio. The jet stretch minus ratio is generally accepted as a comprehensive index of the rheology and hydrodynamic process of wet spinning. The protofibers prepared by solution polymerization with other experimental parameters kept constant were studied. The effects of apparent minus stretch on the properties of the as-spun fibers are presented in Table II. The effects of apparent minus stretch on the morphologies of the as-spun fibers are shown in Figure 1. The shape of the cross-sections of the protofibers were dumbbell- to the oval-shaped, but the cross-section gave no apparent evidence of a clear pore structure. The tensile strengths increased from 0.541 to 0.592 cN/dtex. Also, the densities ranged from 1.130 to 1.144 g/cm^3, with the jet stretch minus rate decreasing from −20 to −55%. This demonstrated that when the protofiber extruded from the spinneret, the initial phase of stretching involved the deformation of the fibrillar structure with concurrent orientation of the fibrils. In other words, it appeared that improvement in fiber density in the protofiber also resulted in improvement in the tensile strength of the protofiber.

Figure 2 shows the effects of swelling degree and iodine adsorption on the morphologies of as-spun fibers at different minus stretch ratios, with the jet stretch minus rate decreasing from −55 to −20%. The swelling degree increased from 220 to 280%, and the iodine adsorption increased from 56 to 78%. With the jet stretch minus rate decreasing from −55 to −20%, the time for the coagulation protofiber in the coagulation bath decreased, which resulted in a more loosely packed microstructure in the protofibers, so the porosity also increased and the density decreased.

SEM analysis of the spinning process

To determine the effect of different stretch rates on the fiber properties and its structure, we adjusted the velocity of the spinning solution in the spinneret hole to 287 cm/min and kept this constant for all the fibers. Observations also showed that the internal microscopic structure of the fiber was not significantly affected by the bath temperature. The solvent content in the bath provided a more porous internal structure. Figure 3 shows the SEM of the longitudinal surface morphology [Fig. 3(A)] and the cross-sections [Fig. 3(B)] of the wet-spun fibers, which were attained from different bath variables. The ratio of the final length of the drawn sample to its original length increased from 1 to 4.5. The diameter of fibers decreased, and their surfaces became smoother. The reduction of the diameter of the fibers was attributed to the draw ratio increases, which caused the chain orientation to change, whereas the smoothness of the surface of fibers at higher draw ratios depended on the possibility of cavity healing, which was filled by solvent and nonsolvent in the coagulation bath. Figure 3(a–c) shows the effect of the solvent content in three coagulations baths on the internal structures; the micrographs demonstrate a significant increase in the porosity of the fibers. This was particularly evident in the fibers obtained from the wet-spinning choice because when there was more solvent in the bath, the residual solvent in the fiber was higher without a change in the run time

TABLE III
Mechanical Properties of the Fibers Produced by the Different Processes

Process	Fiber diameter (μm)	Cross-section	Average number of voids per fiber cross-section	Protofiber bulk density (g/cm^3)	Elongation at break (%)	Titer (dtex)	Tenacity (cN/dtex)
a	34	Bean	17	1.136	154.6	4.12	2.17
b	27	Bean	16	1.140	149.2	3.89	2.56
c	23	Bean	14	1.140	145.8	3.55	3.12
d	22	Bean	14	1.142	134.5	3.25	3.45
e	18	Bean	16	1.155	121.2	2.89	5.34
f	17	Round	6	1.166	25.8	2.78	7.20
g	12	Round	5	1.168	14.5	1.12	8.23

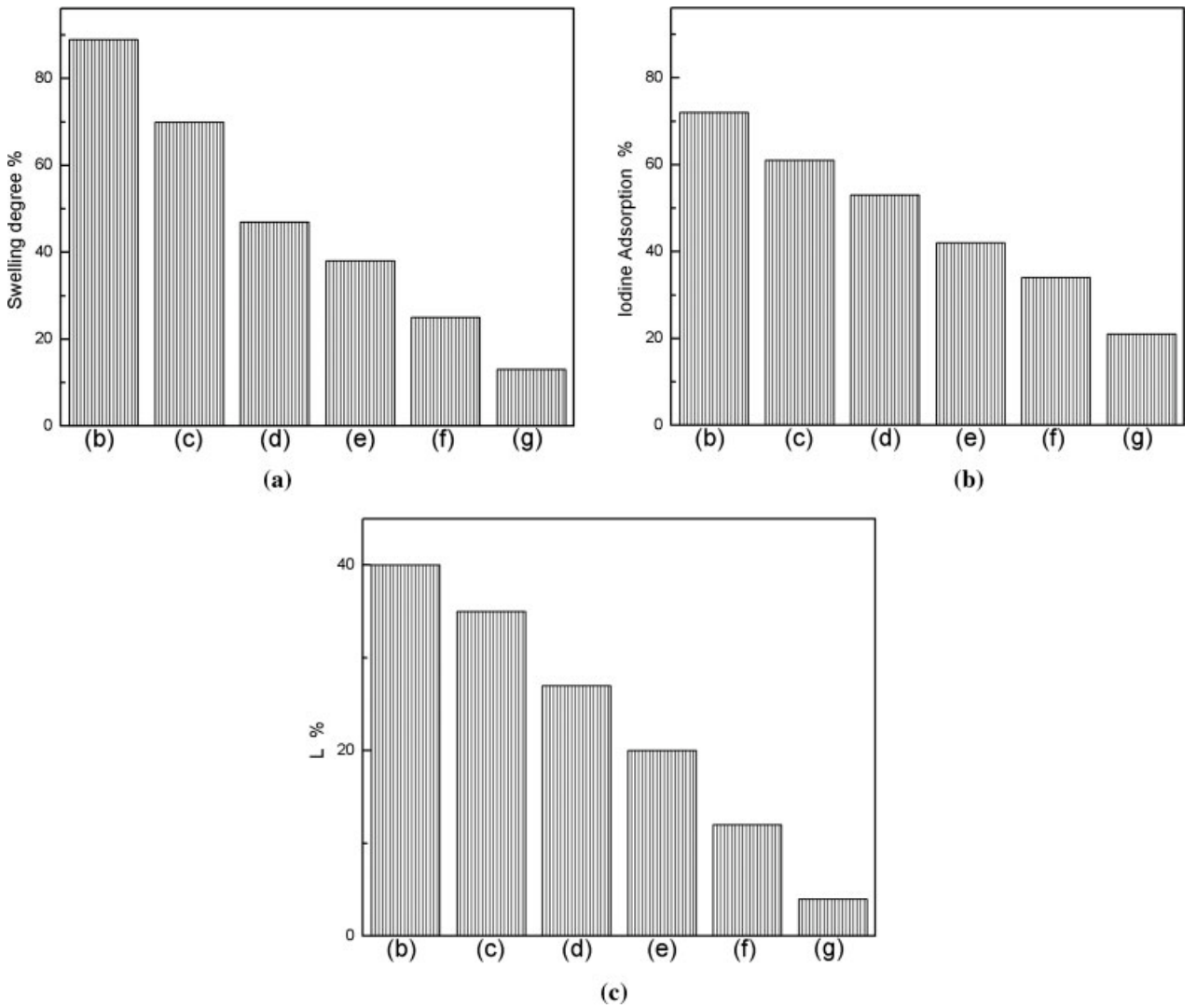

Figure 4 Effect of (a) swelling degree, (b) iodine adsorption, and (c) ΔL on the morphology of as-spun fibers at different drawing ratios.

in the bath. Presumably, the water could not wash out all the residual solvent; in the subsequent drying operation, the residual solvent acted as a strong swelling agent to the fiber, particularly at temperatures as high as 95°C. Some voids were created in the fiber due to the swelling effect. At the same time, with a soft, flexible structure, in a subsequent stretching baths, the molecular chains were able to straighten out more easily along the fiber axis. However, a more effective orientation of the fiber came into being during the second and third bath stretching; thus, the fiber attained a more perfectly developed oriented structure. In the subsequent washing and drying operations, as shown in Figure 3(d–g), the mechanical properties of the fibers (presented in Table III) changed to some extent in the different processes. The bulk density of protofibers increased from 1.142 g/cm^3 in the washing bath at 60°C to 1.168 g/cm^3 in the steam stretch machine at 160°C. The average number of voids per fiber cross-section decreased from

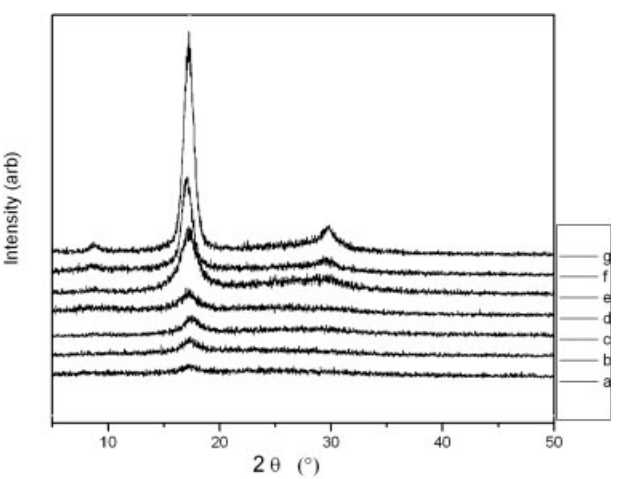

Figure 5 X-ray diffractograms of wet-spun PAN fibers with various draw ratios: (a) minus stretch $\lambda_0 = -0.5$, (b) $\lambda_1 = 1.5$, (c) $\lambda_2 = 1.5$, (d) $\lambda_3 = 1.2$, (e) $\lambda_4 = 1.9$, (f) $\lambda_5 = 1.1$, (g) $\lambda_6 = 2.75$.

TABLE IV
Parameters of the Reflections of PAN Fibers in Different Stretch-Ratio Processes

Drawing process	Diffraction angle (°)	*d*-spacing (Å)	Crystal size (Å)	Peak width at half-maximum (°)	Crystallinity (%)	Crystallite orientation factor
a	16.980	5.1393	32.25	2.52	45	0.57
b	16.990	5.1452	34.58	2.34	47	0.61
c	17.202	5.1324	37.29	2.28	50	0.68
d	16.940	5.1512	45.87	2.20	57	0.70
e	16.894	5,1438	52.13	1.86	62	0.72
f	17.007	5.1571	59.45	1.52	65	0.81
g	17.126	5.1346	62.47	1.33	67	0.85

17 in process a to 5 in process g. As the fibers were drawn, especially at collapse temperatures above the macromolecular glass-transition temperature with the aqueous vapor, this stage had no profound effect on the thermolysis cyclization of side cyan group. The microvoids presenting on the fibers collapsed, and more compact structures were formed. At the same time, the drawing processes of the fibers oriented the molecular chains, which resulted in the improvement of tenacity, which increased from 3.45 to 8.23 CN/dtex; however, the elongation at break decreased from 134.5% in process d to 14.5% in process g.

Figure 4 shows the effect of swelling degree, iodine adsorption, and ΔL on the as-spun fibers with different drawing ratios. As the drawing process went on, the swelling degree, iodine adsorption, and ΔL of the as-spun fibers decreased. At the same time, the porosity decreased and became more compact, which resulted in the drawing of the fibers being oriented along the molecular chains and the improvement of the mechanical properties, as shown in Table III.

Crystalline structure and molecular orientation

XRD has been often used to investigate the crystalline structure and molecular orientation of fiber materials. To determine the crystalline characteristics and molecular orientation of these fibers more precisely, 2θ and an azimuthal scan were performed. Figure 5 shows the X-ray diffractograms of the filaments with different draw ratios. Regardless of the draw ratio, all PAN fibers showed a characteristic sheet crystallinity,[6] an intensive peak at $2\theta = 17^\circ$ for the (101) hexagonal lattice plane.[18] Moreover, the half-width at maximum intensity of the X-ray diffractogram increased gradually with increasing draw ratio. These results show that the preferred orientations of the crystalline regions are aligned along the fiber axis as the draw ratio varies. The new appearance and intensity of crystalline peaks at 29°for the (020) lattice plane revealed that the PAN fibers had a developed crystalline structure and a high crystallinity. Moreover, the crystalline structures of the PAN fibers were affected by drawing in the range from e to g, as shown in Figure 5; that is, an orientation-induced crystallization occurred with stretching in the case of the wet-spun PAN fibers. So, the origin of high drawability depended on the basis of the chain orientation and the spinning process. The Bragg spacing (*d*-spacing) and other parameters are shown in Table IV; the half width decreased and *L* increased as the draw ratio was varied, but the *d*-spacing did not change. The drawing process only affected the crystallinity and not the crystalline structure.

To investigate the molecular orientation in the crystalline and amorphous regions, we performed an azimuthal scan on the XRD fiber patterns. The crystalline orientation was examined at $2\theta = 16.5$–17.2°, which well reflected sheet crystallinity. For the crystalline orientation (Fig. 6), as the draw ratio increased, peak intensities at 90° increased, which corresponded to the orientation along the fiber axis; that is, a preferential chain orientation occurred in the crystalline region on drawing. However, the degree of orientation of the PAN fibers in the crystalline region was somewhat low. The intensity and width for a peak are related to the degree of orientation. Therefore, to investigate the degree of orientation of the PAN fibers in detail, the orientation coefficient was determined quantitatively on the basis of the Herman's orientation factor (in Table IV). An increase

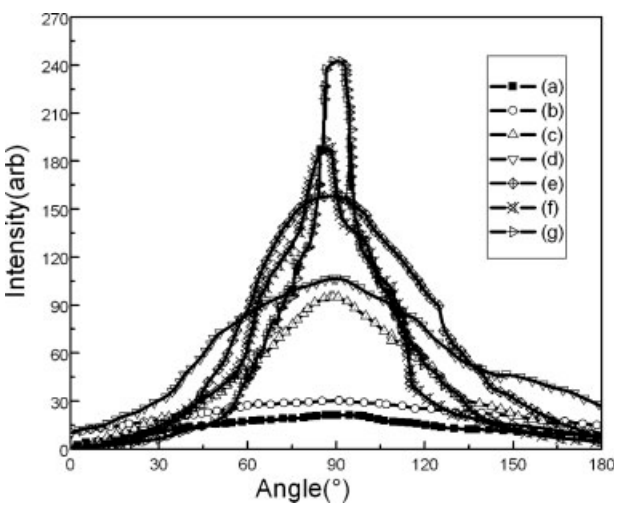

Figure 6 Azimuthal scan of the PAN fibers with various draw ratios in the crystalline region ($2\theta = 17^\circ$).

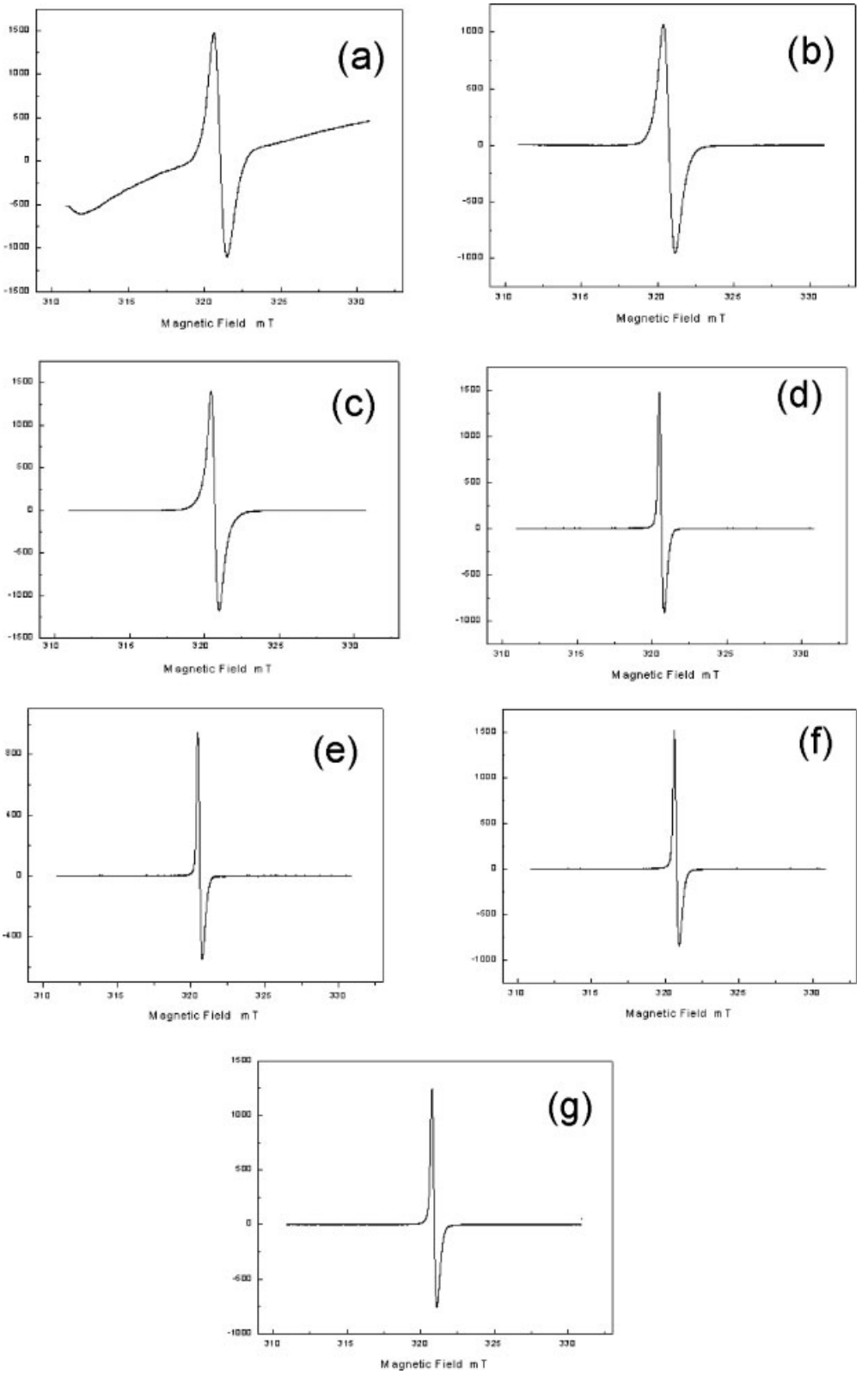

Figure 7 ESR patterns of the fibers in different draw processes as measured at 303 K.

in the orientation coefficient was observed for the PAN fibers with increasing draw ratio.

In addition, processes a and b had a lower degree of orientation and, consequently, a very low amorphous orientation coefficient value. The small drawing effect allowed the molecular chain in the amorphous region to be fully oriented; thus, a maximum amorphous orientation could be achieved with a

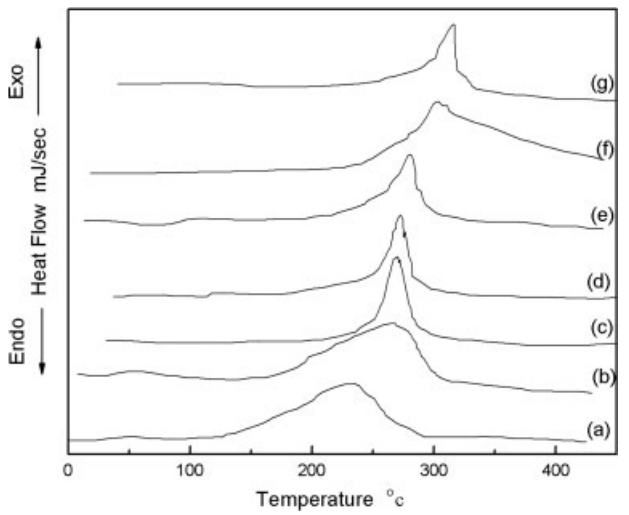

Figure 8 DSC thermograms of the PAN fibers in different draw ratio processes.

small mechanical force, which was the tension required to keep the filament from not being contracted. These results indicate that molecules in the amorphous regions were easily oriented by small amounts of force but were well oriented to the direction of external force. It appears that two different types of tensile behaviors were associated with different molecular orientations. The molecular orientation of the PAN fibers abruptly increased above $\lambda_1\lambda_2\lambda_3 = 2.7$. The difference in tensile behavior dependent on the draw ratio was attributed to the molecular orientations of the PAN fibers (as shown in Table IV).

ESR structural changes

The interactions of nitrile groups in the AN component as a dominant factor in the chain conformations certainly contributed to the foregoing characteristics, so ESR was proven to be sensitive to local morphology and segmental dynamics. Typical ESR spectra for the PAN fibers in different drawing processes at room temperature are presented in Figure 7. These were mainly due to steric and polar interactions between adjacent monomeric units.[33] At the beginning, the spectra were characteristic of the presence of multiple radicals. The *G* (Gaussian) values for process a were the largest, which was due to the very stiff polymer chains as a consequence of dominant interactions of nitrile groups along the chains. The intrachain and interchain hydrogen bonding between DMSO and AN could facilitate the dissipation of absorbed energy without bond breakages taking place, and this was lost to some extent when AN units were incorporated within the polymer chains. As the drawing process went on, it decreased gradually. The PAN fibers were washed and dried, so DMSO was removed until the content for DMSO in PAN fibers was below 100 ppm. At last, the quartet splitting became smaller. This was clearly dominated by the presence of the chain radical of AN. The larger half-width at half-height of low-field and high-field process a compared to process g were ascribed to a more heterogeneous environment caused by the sequence structure.

Thermal and mechanical properties

Figure 8 presents DSC thermograms of PAN fibers at different drawing processes. The various parameters obtained from these exotherms, namely, initiation temperature (T_i), peak temperature (T_p), termination temperature (T_t), difference between T_i and T_t, and evolved heat (ΔH), are tabulated in Table V. Some chemical changes resulting from oxidization and cyclization were characterized by these exothermic peaks. Processes a and b exhibited main exothermic peaks at 239.3 and at 274.5°C, respectively, with shoulders. For the drawn filament, the shoulder peak disappeared, and the major exothermic peak shifted to a slightly higher temperature as the draw ratio increased. This implied that the molecular orientation caused the thermal degradation of PAN molecules, although not significantly. It also indicated that the size and shape of the exotherm and heat liberated during the scan were strongly dependent on the morphology and physical changes occurring during fiber processing. This clearly shows that the initiation of one of the reactions, that is, the preceding one, did have a significant effect on the orientational stretching.

CONCLUSIONS

The process of fiber formation under continuous spinning conditions was determined by jet stretch minus ratio. The improvement in fiber density in the protofibers also resulted in increments in the tensile strength of the protofiber. The time for the protofiber in the coagulation bath decreased, which resulted in a more loosely packed microstructure of the protofiber. The drawing of the fibers oriented the molecu-

TABLE V
Parameters Obtained from DSC Exotherms of PAN in Different Draw-Ratio Processes

Serial number	T_i (°C)	T_t (°C)	ΔT (°C)	T_p (°C)	ΔH (J/g)
a	134.5	239.3	287.8	153.3	983
b	157.4	274.5	299.3	141.9	912
c	185.7	275.4	290.2	104.5	784
d	259.3	277.2	293.3	34	753
e	271.4	291.3	299.5	28.1	652
f	280.3	301.2	309.2	28.9	451
g	294.5	310.1	317.8	23.3	432

ΔT, $T_i + T_p$.

lar chains, which resulted in an improvement in tenacity. The porosity decreased and became more compact, which resulted in an improvement in the mechanical properties. The half-width decreased and L increased with draw ratio, but the d-spacing did not change. The drawing caused only the crystallinity rather than the crystalline structure. The water could not wash out all the residual solvent during the three stages. In the subsequent drying operation, the residual solvent acted as a strong swelling agent for the fibers. The larger half-width at half-height of low field and high field was ascribed to a more heterogeneous environment caused by the sequence structure. The size and shape of the exotherm and heat liberated during the scan were strongly dependent on the morphology and physical changes occurring during fiber making.

References

1. Kim, H. S.; Shioya, M.; Takaku, A. J Mater Sci 1999, 34, 3299.
2. Kim, H. S.; Shioya, M.; Takaku, A. Mater Sci 1999, 34, 3307.
3. Sen, K.; Bahrami, S. H.; Bajaj, P. J Macromol Sci Rev Macromol Chem Phys 1996, 36, 1.
4. Bajaj, P.; Sreekumar, T.; Sen, V. K. J Appl Polym Sci 2002, 86, 783.
5. Jain, M. K.; Abhiraman, A. S. J Mater Sci 1987, 22, 278.
6. Balasubramanian, M.; Jain, M. K.; Bhattacharya, S. K.; Abhiraman, A. S. J Mater Sci 1987, 22, 3864.
7. Jain, M. K.; Balasubramanian, M.; Desai, P. J Mater Sci 1987, 22, 301.
8. Liu, C. K. J.; Cuculo, A.; Smith, B. J Polym Sci Part B: Polym Phys 1989, 27, 2493.
9. Paul, D. R. J Appl Polym Sci 1968, 12, 2273.
10. Law, S. J.; Mukhopadhyay, S. K. J Appl Polym Sci 1997, 65, 2131.
11. Stoyanov, A. I. J Appl Polym Sci 1982, 27, 235.
12. White, J. L.; Hancock, T. A. J Appl Polym Sci 1981, 26, 3157.
13. Um, I. C.; Ki, C. S.; Kweon, H. Y.; Lee, K. G.; Ihm, D. W.; Park, Y. H. Int J Biol Macromol 2004, 34, 107.
14. Paul, D. R.; Mcpeters, A. L. J Appl Polym Sci 1977, 21, 1699.
15. Stoyanov, A. I. J Appl Polym Sci 1981, 26, 1813.
16. Doppert, H. C.; Harmsen, G. J. J Appl Polym Sci 1973, 17, 893.
17. Paul, D. R. J Appl Polym Sci 1969, 13, 817.
18. Liu, X. D.; Ruland, W. Macromolecules 1993, 26, 3030.
19. Sokot, M.; Grobelny, J.; Turska, E. Polymer 1987, 28, 843.
20. Bashir, Z.; Tipping, R.; Church, S. P. Polym Int 1994, 33, 9.
21. Paul, D. R.; Mcpeters, A. L. J Appl Polym Sci 1973, 21, 1669.
22. Paul, D. R. J Appl Polym Sci 1968, 12, 383.
23. Han, C. D.; Segal, L. J Appl Polym Sci 1970, 14, 2999.
24. Fujiwara, H.; Shibayama, M.; Chen, J. H.; Nomura, S. J Appl Polym Sci 1989, 37, 1403.
25. Prased, G. Synth Fibers 1985, 1/3, 6.
26. Han, C. D.; Segal, L. J Appl Polym Sci 1970, 14, 2973.
27. Paul, D. R.; Armstrong, A. A. J Appl Polym Sci 1973, 17, 1269.
28. Rakas, M. A.; Farris, R. J. J Appl Polym Sci 1990, 40, 823.
29. Imai, Y. J Appl Polym Sci 1970, 14, 225.
30. Jr, W. D.; Clair, A. S. J Appl Polym Sci 1991, 43, 501.
31. Dave, V.; Glasser, W. G.; Wilkes, G. L. J Appl Polym Sci Part B: Polym Phys 1993, 31, 1145.
32. Sen, K.; Bajaj, P.; Sreekumar, T. V. J Polym Sci Part B: Polym Phys 2003, 41, 2949.
33. Andreis, M.; Rakvin, B.; Veksli, Z.; Rogosic, M.; Mencer, H. J. Polymer 1999, 40, 1955.